

Supporting Information

Infant Diapers Waste Derived Multifunctional MoN-Ni₃C@CFs for Full Water Splitting in Neutral and Alkaline-pH and Solar-to-Hydrogen Conversion: A Win-Win Cooperation

Jayaraman Jayabharathi*, **Thanikachalam Akshy#**, **Dhanasingh Thiruvengadam**, **Ravichandran Nithiasri**, **Arokiadoss Davidrichetson** and **Mayakrishnan Raj kumar**

*Department of Chemistry, Materials science lab, Annamalai University, Annamalai nagar, Tamilnadu 608002, India. *jtchalam2005@yahoo.co.in*

#Department of General Medicine, Saveetha Medical College, Thandalam, Chennai, Tamilnadu 602105

Contents

SI-I. Experimental Section

SI-II. Calculations

SI-III. Figures

SI-IV. Tables

SI-I. Experimental Section

S1-E1. Materials

Urinary diaper collected from Chidambaram Government hospital. Nickel nitrate hexahydrate and ammonium molybdate was received from SISCO CHEM. Nickel Foam (NF) received from Vitra Technologies, India. Iridium oxide (IrO_2), platinum derived carbon (Pt-C), Nafion 15% and alumina mesh received from Sigma Aldrich. All chemicals used as received without any further purification. The Deionized water was used throughout the experiment.

S1-E2. Characterization of an electrocatalyst

High resolution transmission electron microscopy (HR-TEM) conducted on a JEOL JEM 2200FS microscope operated at 200 kV acceleration voltage, probe-side C_s -corrected, integrated with an Oxford X Max 100 Energy Dispersive X-ray (EDX) detector. Field Emission Scanning Electron Microscopy (FE-SEM) was conducted on ZEISS oxford and an accelerated voltage at 3 kV with the measurement of EDX. Structural interpretation of CoO_x -Bo identified with x-ray diffraction (XRD), were taken on a powder diffractometer (Rigaku, D/MAX, 2500 V) with $\text{Cu K}\alpha$ radiation ($\lambda=1.54056 \text{ \AA}$) operating at 40 KV and 250 mA. Chemical bond structure identified based on Fourier Transform Infrared (FT-IR) spectrometer Thermo Nicolet 6700. Raman measurement was carried out at room temperature, and the signals were recorded by using Raman spectroscopy (Renishaw) with a 514.5 nm laser excitation. XPS measurements were carried out in an ultra-high vacuum (UHV) set-up equipped with a monochromatic $\text{Al K}\alpha$ X-ray source (1486.6 eV; anode operating at 12.25 kV and 300 W) and a high resolution Phoibos 150 MCD analyzer (SPECS). X-ray photoemission spectra were measured in fixed analyzer transmission mode with pass energy 20 eV and step size 0.5 and 0.05 eV for survey and region scans correspondingly.

S1-E3. Electrode preparation and characterization

All electrochemical measurements were carried out on a Biologic SP-300 Potentiostat electrochemical workstation, the linear sweep voltammogram (LSV) test was carried out in 1 M KOH electrolyte with a scan rate of 10 mV/s three-electrode setup. To prepare catalyst ink, 0.5 mg of the as-prepared MoN-Ni₃C@CFs was evenly dispersed in 0.5 mL of propanol, and then the as-obtained solution was treated with ultrasound for 20 min. For comparison, a 0.005 mg/ml commercial IrO₂ and Pt/C suspension was made using a comparable methodology. Before coating, the NF was washed with acetone, HCl aqueous solution, deionized water and ethanol in sequence. In a three-electrode setup nickel foam (NF) as the working electrode, Ag/AgCl (3 M KCl) as reference electrode, and a platinum wire as counter electrode. Measured potentials were referred to the reversible hydrogen electrode (RHE) $E_{\text{RHE}} = E_{\text{Ag/AgCl}} + 0.923 \text{ V}$. The resistances of as prepared electrocatalysts were acquired from EIS tests at the overpotential of different mV (vs. RHE) in the frequency scope of 100 kHz to 10 mHz. The durability was tested by cyclic voltammetry (CV) and current-time (i-t) curve tests.

SI-II. Calculations

SI.C1. Calculation of Overpotential (η)

The overpotential (η) was determined according to the formula: $\eta \text{ (V)} = E \text{ (RHE)} - 1.23 \text{ V}$

SI.C2. Calculation of Tafel slope

Tafel plots were derived from the LSV curves and the Tafel slope was calculated using the equation: $\eta = a + b \log J$, where η –overpotential, a - exchange current density, b -Tafel slope and j - corresponding current density (mA /cm²) as well as Tafel constant

SI.C3. Calculation of ECSA

The calculations of ECSA and roughness factor (RF) are based on the following equation: $\text{ECSA} = C_{\text{dl}} / C_s$; $\text{RF} = \text{ECSA} / \text{GSA}$, where C_{dl} - double layer capacitance of catalyst in 1.0 M

KOH (mF) and C_s - specific capacitance of the catalyst ($C_s = 0.04 \text{ mF cm}^{-2}$ in 1.0 M KOH). In eq (5), RF - roughness factor and GSA - geometric surface area of the material.

SI.C4. Calculation of Faradaic Efficiency (FE) from RRDE

The Faradaic Efficiency for MoN-Ni₃C@CFs in OER process was calculated by using Rotating Ring-Disk (RRD) technique as follows:

Ring current (I_{ring}) = 0.0405 mA

Disc current (I_{disc}) = 0.0.1821 mA

Collection Efficiency (N) = 0.246 (The Collection Efficiency (N) value calculated experimentally by using ferri/ferrocyanide system in 0.1 M KCl with 10 mM K₃[Fe(CN)₆], the data are given Table)

S.No	Rotation speed (RPM)	Disc current (mA)	Ring current (mA)	Collection Efficiency (N)
1	300	0.24005	0.052704	0.21756037
2	600	0.25710	0.069794	0.27146635
3	900	0.39250	0.084198	0.21451719
4	1200	0.41204	0.096619	0.23448937
5	1500	0.57801	0.10751	0.18600024
Average				0.2398067044

Faradaic Efficiency in of OER process: $I_{ring}N * I_{disc} * 100$

$$: 0.93056 * 100 = 93.05 \%$$

SI.C5. Determination of energy consumption

With the CVs results, we can obtain the apparent activation energy (E_a) calculated using the Arrhenius equation: $\ln j = -E_a/RT + b$, where j- current density, R-gas constant, T-Temperature and b-slope

SI.C6. Determination of number of active sites

For MoN-Ni₃C@CFs:

Area under NiOOH formation peak = $5.97 \times 10^{-5} \text{ AV}$

Charge associated with FeOOH formation = $5.97 \times 10^{-5} \text{ AV} / 0.005 \text{ V s}^{-1}$

$$\text{Charge of an electron} = 1.602 \times 10^{-19} \text{ C}$$

$$\text{Number of electrons transferred} = 7.45 \times 10^{16}$$

Since, MoN-Ni₃C@CFs to NiOOH formation reaction is a single electron transfer reaction, the number of electron transferred during the reaction is equal to the number of M-sites involved in the reaction.

$$\text{Hence, Number of M-sites involved in OER} = 10.563 \times 10^{-3} \text{ C}$$

SI.C7. Surface coverage of Ni²⁺/Ni³⁺ (Γ*)

The surface coverage of the Ni(OH)₂/NiOOH redox species in Ni@Ni₃C/FAC-K can be evaluated based on the following equation: $I_p = (n^2 F^2 / 4RT) \Gamma^*$, where I_p , n , F , R , T , v , A and Γ^* are peak current, number of transferred electron, Faraday (96,845 C mol⁻¹), ideal gas constant (8.314 J K⁻¹ mol⁻¹), temperature (298 K), the potential scan rate, geometric surface area of glassy carbon electrode (0.0706 cm²) and the surface coverage of the redox species, respectively.

$$\text{Anodic value: slope} = 0.087 = (n^2 F^2 / 4RT) \Gamma^* = 946385.6 \Gamma^*, \Gamma \Gamma^* = 1.17 \times 10^{-7} \text{ mol cm}^{-2}.$$

$$\text{Cathodic value: slope} = 0.098 = 946385.6 \Gamma^*, \Gamma^* = 1.11 \times 10^{-7} \text{ mol cm}^{-2}.$$

SI.C8. Calculation of Turnover frequency (TOF)

The TOF is defined as the number of H₂ or O₂ molecules evolved per active site per second.

TOF of O₂ or H₂ = $TOF = i \frac{S_{geo}}{4Fm}$, where, where j , S_{geo} , F , and m signified current density (mA/cm²), geometric surface area (cm²) of the working electrode, Faraday constant (96,485 C/mol) and moles of the active catalyst species, respectively. For TOF analysis, determination of concentration (m) of surface active species is a major challenge. Finding the position of active centers can provide the necessary guidance to determine m [2].

SI.C9. Active site density

To know the active site concentration, i versus $v^{1/2}$ was plotted using the following equation

$$i = \pm 0.436nFA_{real}C\sqrt{nFDv/RT}$$

The number of active sites is attributed by ($A_{real}C$), where A_{real} and C refer to total electrochemical area and active site concentration, respectively. The C , D , and A_{real} manifest the per-site concentration, diffusion constant and electrochemical area, respectively. The active site density was calculated by considering $D = 1$ and $n = 1$

SI.C10. Proton reaction order (ρ_{RHE})

The proton reaction order (ρ_{RHE}) was determined from the following relation

$$\rho_{RHE} = \left(\frac{\partial \log(i)}{\partial pH}\right)_E = -\left(\frac{\partial E}{\partial pH}\right)_i / \left(\frac{\partial E}{\partial \log(i)}\right)_{pH}, \text{ where } \rho_{RHE} \text{ is the proton reaction order on the RHE scale [3].}$$

SI.C11. The dependency of current on several parameters

For alkaline OER process, current (j) can be written as

$$i = [OH^-] \cdot \theta \cdot e^{-\frac{\Delta G}{RT}}, \text{ where } [OH^-] \text{ indicates the concentration of the electrolyte medium and } \theta \text{ is the surface coverage by } *OH \text{ or } *OOH \text{ sites [4].}$$

SI.C12. Calculation of mass Activity

The mass activity (Ag^{-1}) of electrocatalysts was calculated by the equation of:

$$\text{Mass activity} = j/\text{mass loading}$$

SI.C13. Nature of the charge storage process

Identifying the position of the catalytically active centers in the catalyst by using the following mathematical expression can provide the necessary guidance to accurately determine m

$$i = a\nu^b, \log i = \log a + b \log \nu, \text{ b value was calculated from the log(current) versus log(scan rate) plot, where } i \text{ and } \nu \text{ denote the current and scan rate, respectively. For } b \sim 0.5, \text{ the ion intercalation (diffusion) mechanism predominates, indicating that majority of the active sites are at the interlayer spacing, while a surface-controlled process is expected for } b \sim 1 \text{ [1,2]}$$

SI.C14. Calculation of specific activity

The specific activity ($\text{mA}/\text{cm}^2_{\text{ECSA}}$) of electrocatalysts was calculated by the equation of:

$$(i) \text{ Specific activity} = j/10 \times \text{ECSA}_{\text{BET}} \times \text{amount of loading}$$

$$(ii) \text{ Specific activity} = j/10 \times \text{ECSA}_{\text{Cdl}} \times \text{amount of loading}$$

SI.C15. Calculation of H₂ and O₂ generation

Based on the displaced amount of water due to the hydrogen bubbles the amount of hydrogen generated was calculated using the below relationships.

$$\text{Amount of O}_2 \text{ generated in 1 h} = \text{Amount of water displaced in litres}$$

$$\text{Amount of O}_2 \text{ generated in moles for 1 h} = \frac{\text{Amount of water displaced (liters)}}{22.4 \text{ liters}}$$

The O₂ generation rate was calculated from the electrical charge passed through the electrode using the equation given below.

$$\text{Current obtained during electrolysis} \times \text{Time duration for each potential} = \text{Coulomb}$$

$$\frac{\text{Coulomb} \times F}{96485\text{C}} = \text{No. of moles of } e^- \text{ for H}_2/\text{O}_2 \text{ generation}$$

$$\frac{\text{No. of moles of } e^- \text{ for H}_2 \text{ or O}_2 \text{ generation} \times 1 \text{ mole of H}_2 \text{ or O}_2 \text{ gas}}{4/2 \text{ moles of electron generated}} = \text{Moles of H}_2/\text{O}_2$$

SI.C16. Faradaic efficiency

At the constant potential of 1.64 V given across the MoN-Ni₃C@CFs/NF//MoN-Ni₃C@CFs/NF electrode couples assembled and sealed in H-type full cell in 1.0 M KOH. During the electrolysis, evolved gas molecules were measured by the water displacement method. The applied potential can provide 10 mA cm⁻² current density to the system and the electrolysis was monitored for 60 min. each 10 minutes of analysis data shown in the data (Figure 7b). Theoretical number of moles of gas molecules can be calculated from Faraday's second law of electrolysis according to the following equation: $V_t = Q/nF$, where V_t - number of O₂ molecules calculated theoretically, Q -total charge passed to the cell systems, n -number of electrons ($n=4$ for O₂) and F -Faraday constant 96485.3 C/mol. The Faradaic Efficiency of OER was estimated

using the following equation: $FE = 4Fn_{O_2}/It \times 100\%$, where F is Faraday constant (96485 C/mol), n_{O_2} is the number of moles of experimental O_2 during the reaction (mol), n_{H_2} is the number of moles of experimental H_2 during the reaction (mol), I is the current of the reaction (A), and t is the reaction time (s).

SI.C17. Determination of Power consumption

Based on Faraday's law, power consumption for water electrolysis process can be expressed as follows: Energy consumption ($kWhm^{-3}$) = $V_{cell} \times nF/3600 \times 1/V_m$, where, V_{cell} - voltage during electrolysis, n - number of electrons (4 for OER: 2 for HER), F -Faraday constant of 96,500 C mol⁻¹ and V_m - molar volume of gas to be 24.47 L mol⁻¹ at 25 °C and 1 atm.

SI.C18. Environmental impact assessment

$$\text{Mass Intensity} = \frac{\text{Mass of all reactants used excluding water}}{\text{Mass of product}} \text{kg/kg product}$$

$$\text{Water Intensity (Wp)} = \frac{\text{Mass of all water used}}{\text{Mass of product}} \text{kg/kg product}$$

$$\text{Reaction Mass Efficiency (RME)} = \frac{\text{Mass of product}}{\text{Mass of all reactants}} \times 100\%$$

$$\text{Energy Intensity} = \frac{\text{Amount of non renewable energy used}}{\text{Mass of product}} \text{kW.h/kg}$$

$$E \text{ factor} = \frac{[kg(\text{raw material}) - kg(\text{desired product})]}{[kg(\text{total product including water})]}$$

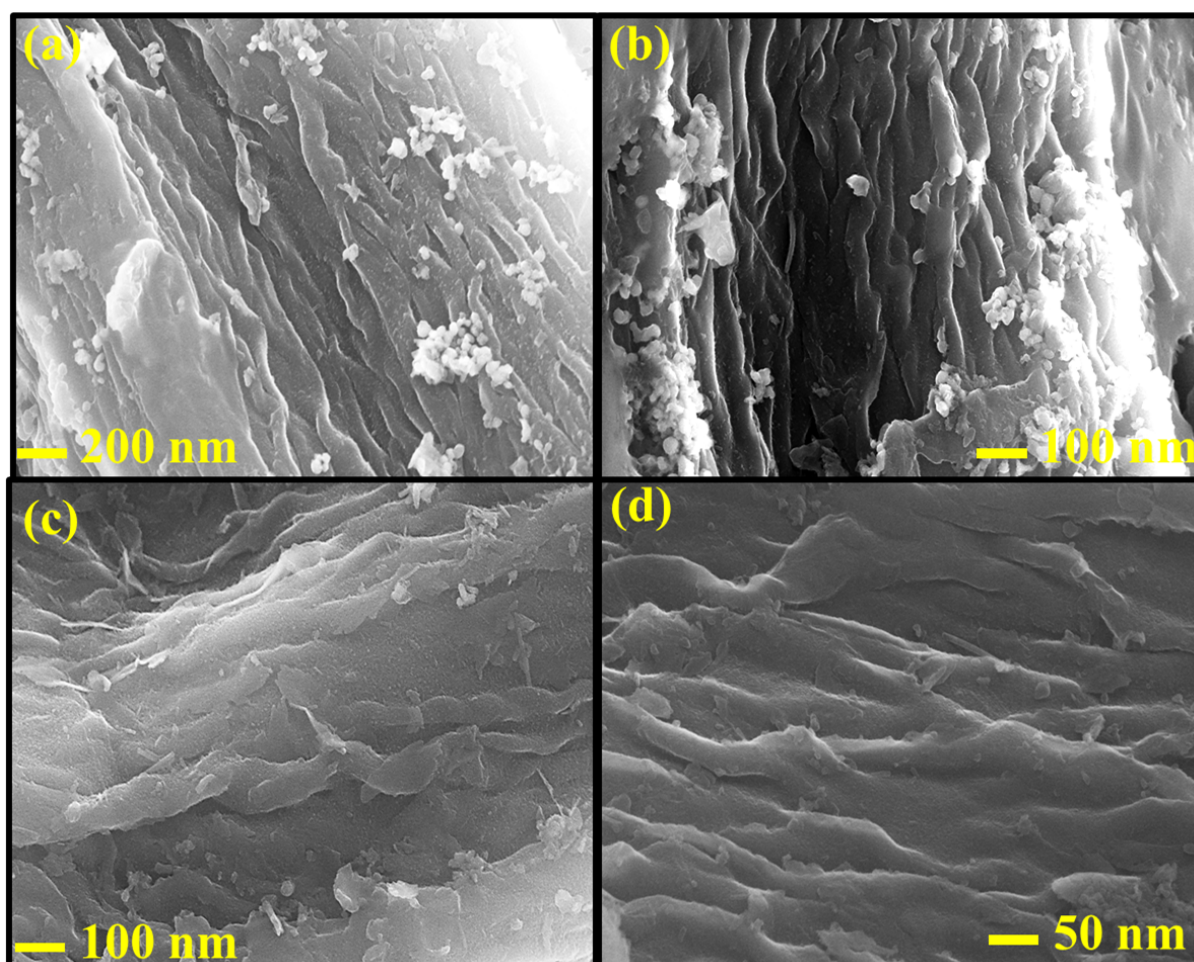
SI-III. Figures**Figure S1. (a, b) FESEM images and (c, d) Horizontal view of banyan roots-like morphology of CFs at various magnification**

Figure S2. Elemental mapping of MoN-Ni₃C@CFs: (a) Mo; (b) Ni; (c) N; (d) C and (e) EDX spectra (inset: Elemental composition)

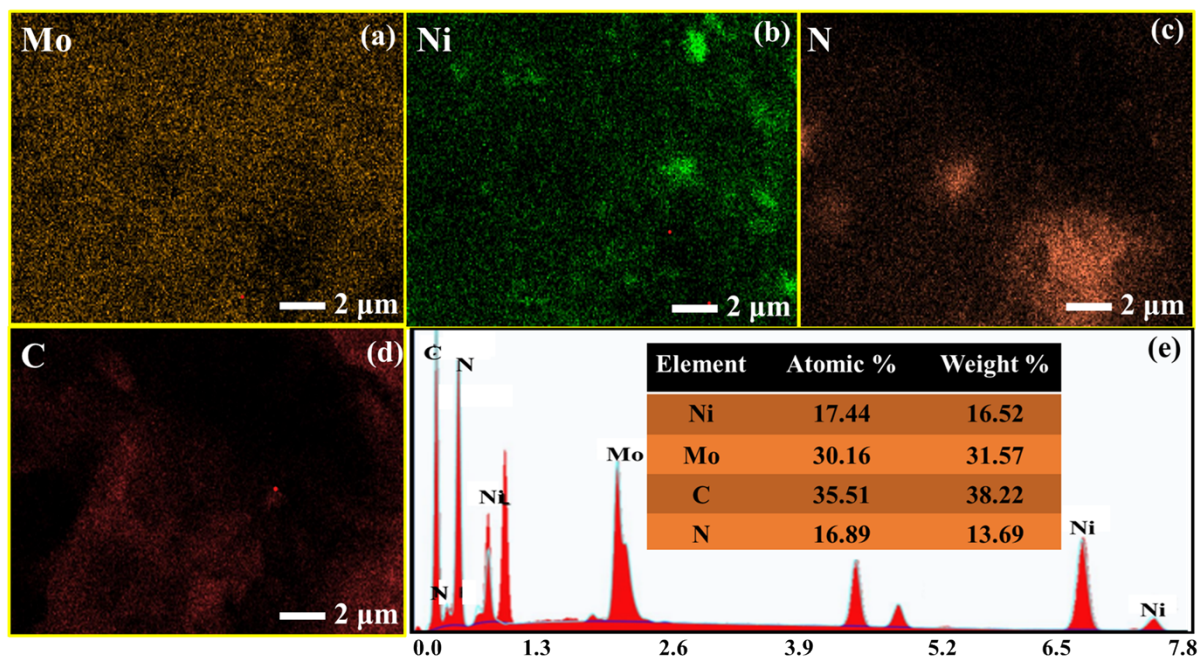


Figure S3. BET surface area analysis: (a,c) N_2 absorption-desorption isotherm plot; (b,d) Pore size distribution of CFs and $NiMoO_4$

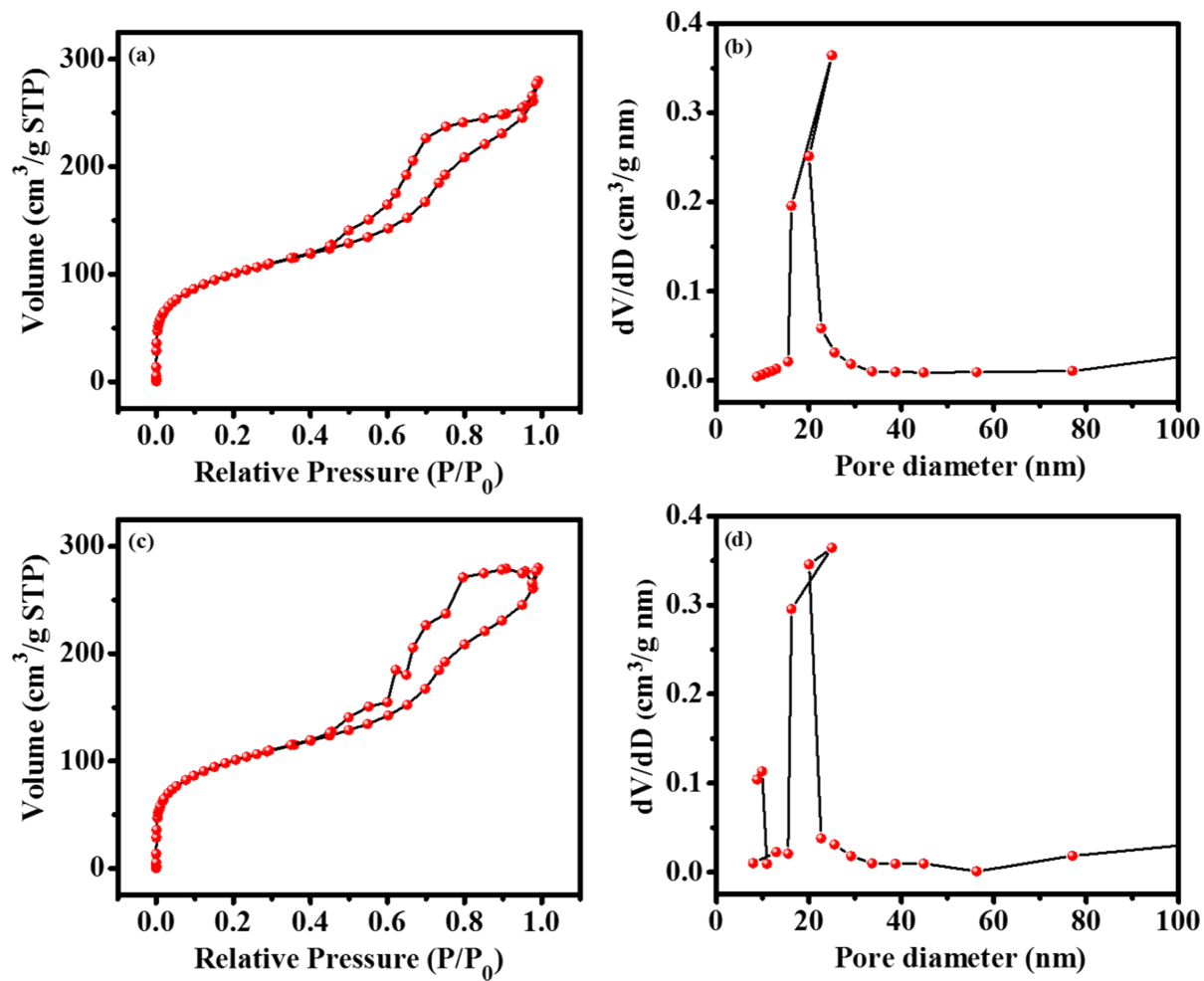


Figure S4. (a) XPS survey spectrum of MoN-Ni₃C@CFs; (b) EPR spectra of MoN-Ni₃C@CFs and NiMoO₄; Overpotential plot @ various current density: (c) OER and (d) HER

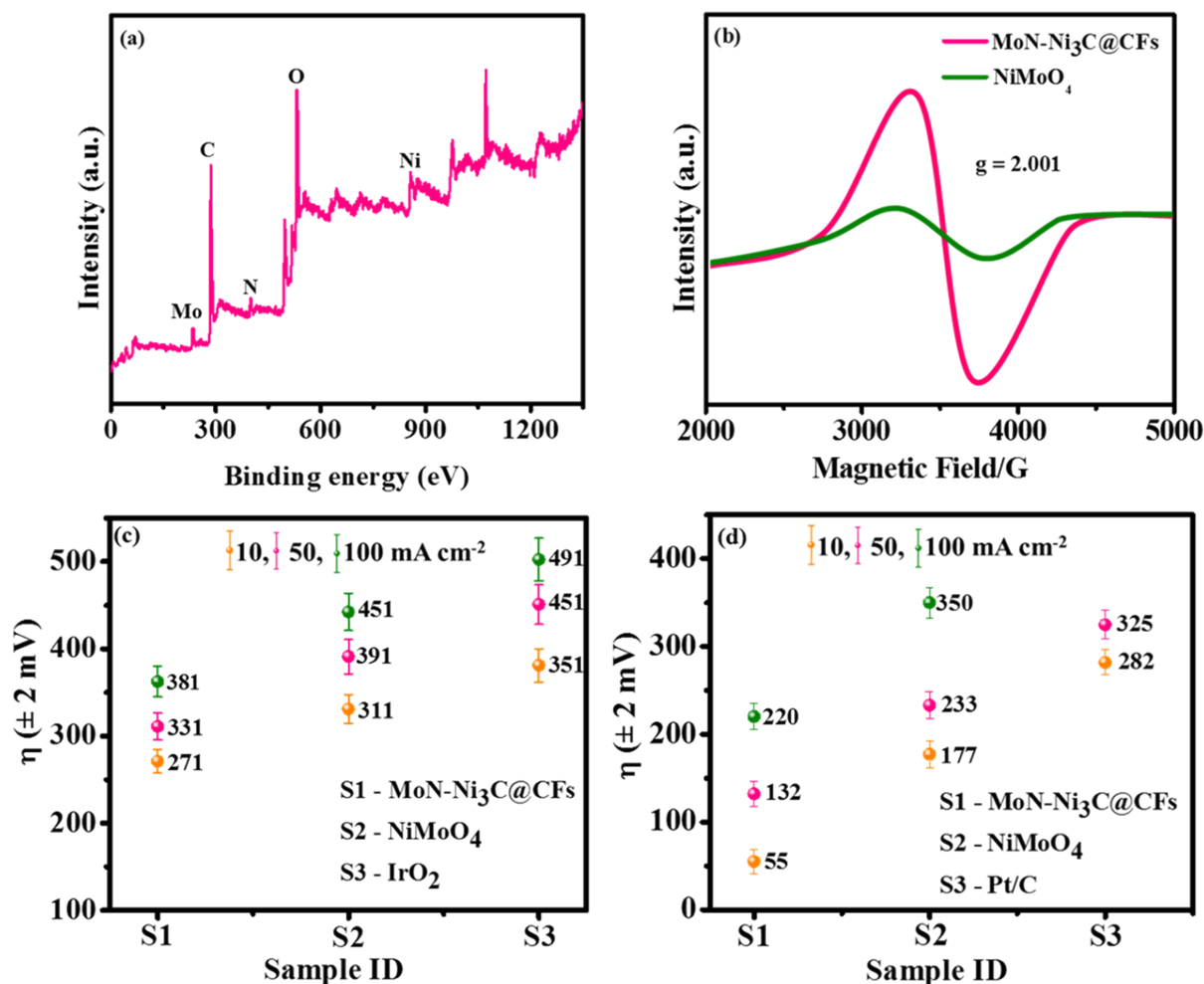


Figure S5. HER performance of carbon-based counter electrodes: (a) LSV curve; (b) Tafel plots and (c) Electrode images

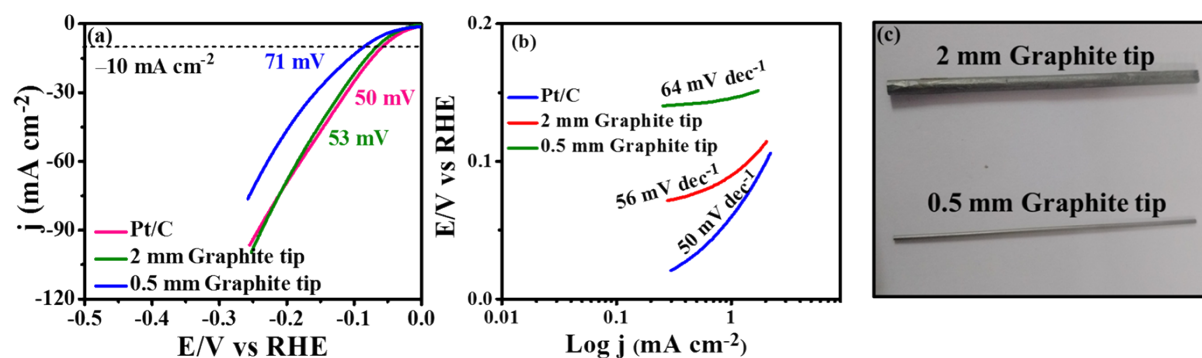


Figure S6. Comparison of LSV curves before and after stability (a) OER; (b) HER; Multi-current process: (c) OER and (d) HER of MoN-Ni₃C@CFs

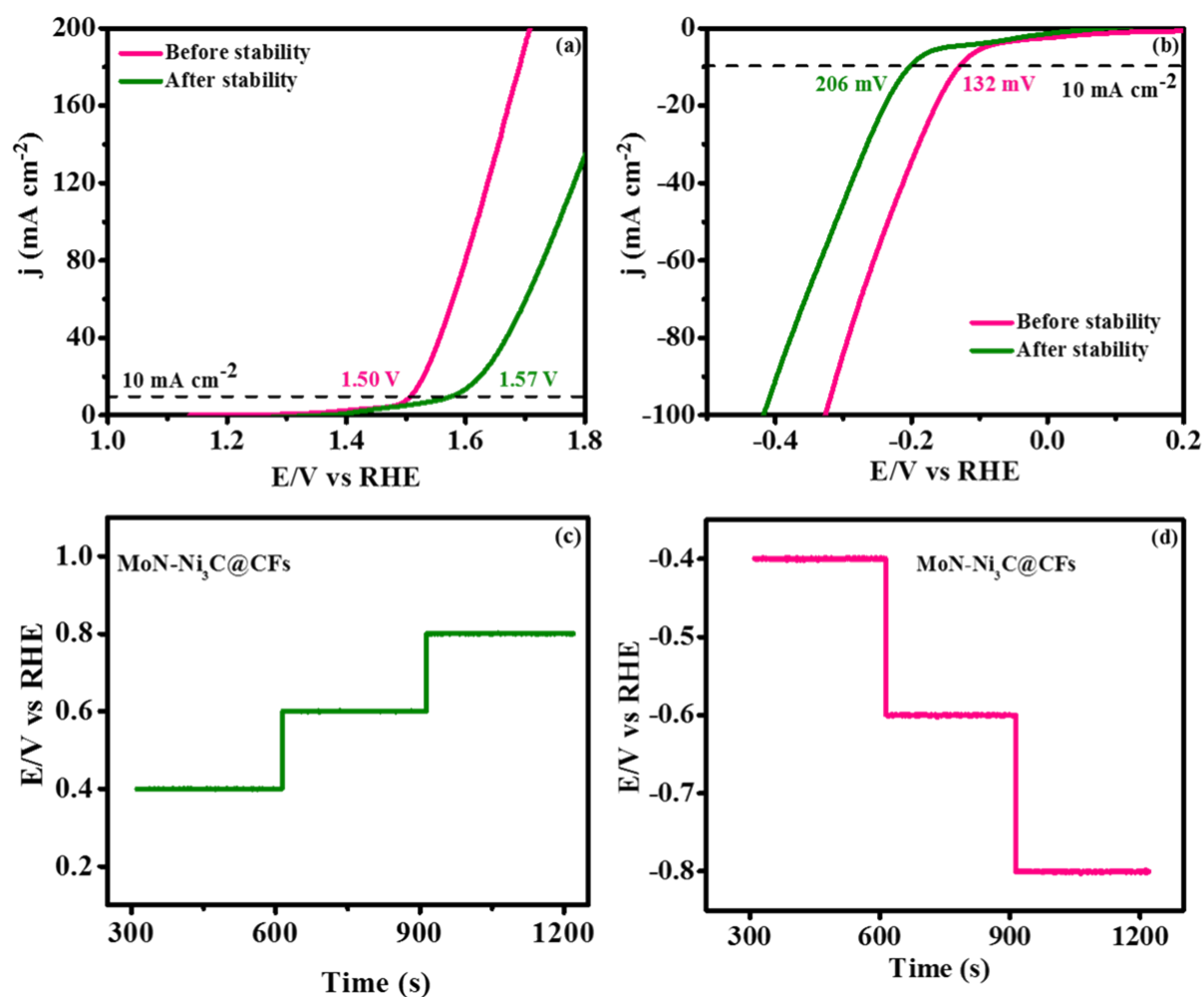


Figure S7. (a) ECSA curve: (a) MoN-Ni₃C@CFs; (b) NiMoO₄; (c) CFs; and (d) Integrated area under LSV curve

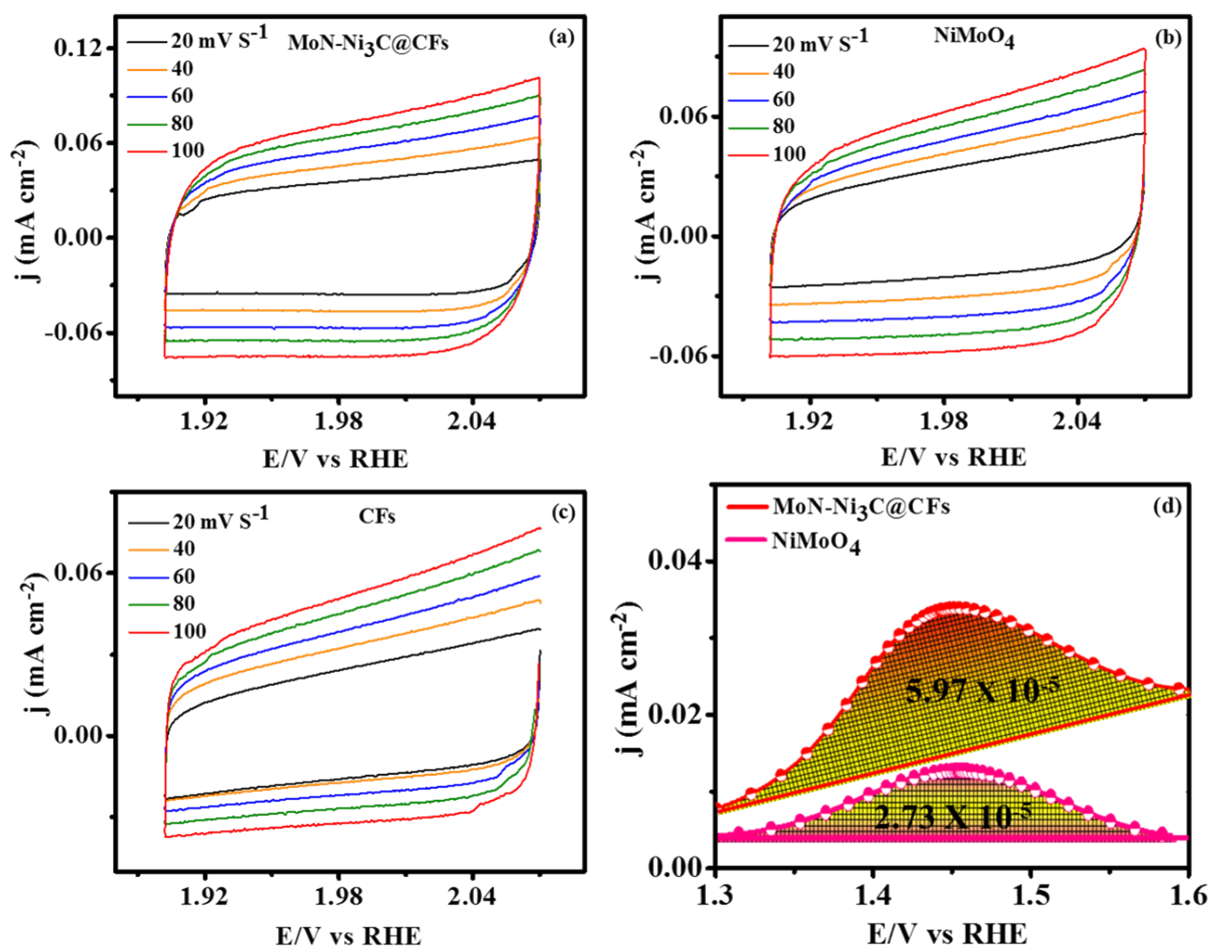


Figure S8.(a) Comparison of LSV curves before and after two electrode stability and (b) Power consumption at various current density

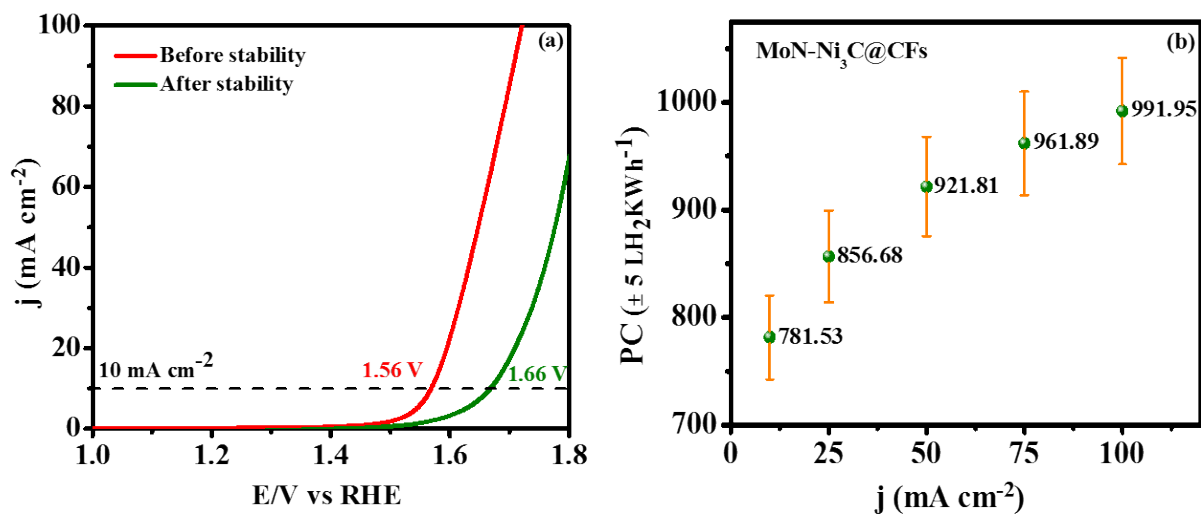


Figure S9. (a) Post- XRD spectrum and (b, c) post- FESEM images of MoN-Ni₃C@CFs

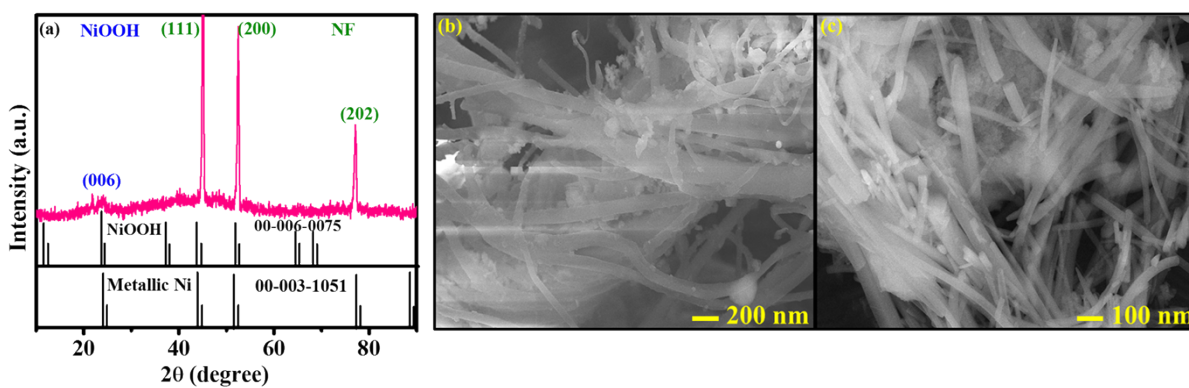


Figure S10. Post FESEM Elemental mapping of MoN-Ni₃C@CFs: (a) Overlay; (b) Ni; (c) Mo; (d) O; (e) C; (f) N and (g) EDX spectra (inset: Elemental composition)

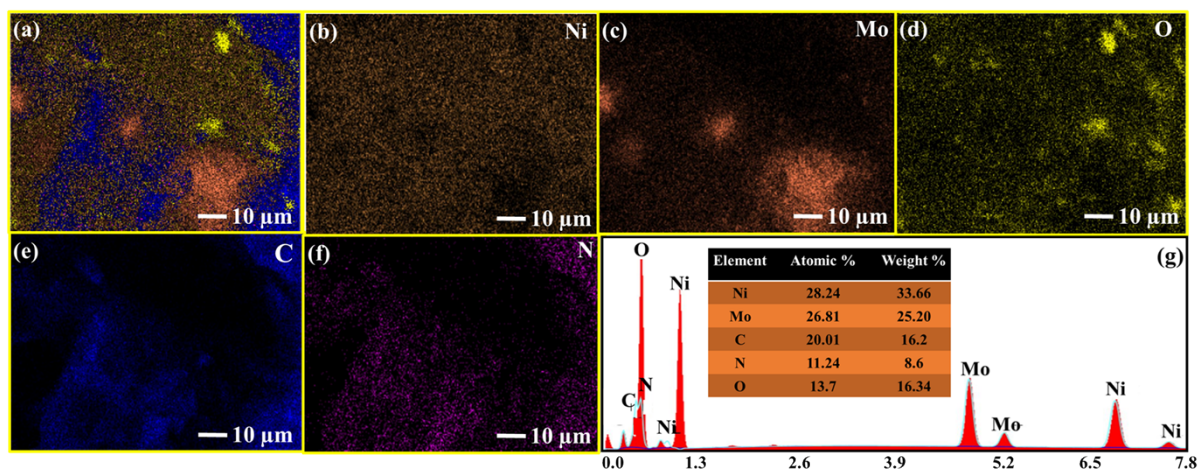
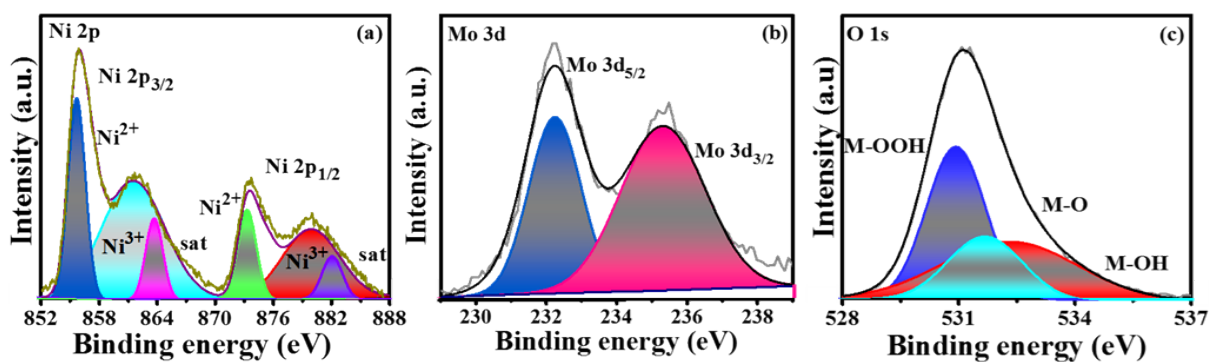


Figure S11. Post-XPS Spectra: (a) Ni; (b) Mo and (c) O of MoN-Ni₃C@CFs



SI-IV. Tables

Table S1. Comparison of OER performance of MoN-Ni₃C@CFs with recently reported transition metal-based catalysts

Catalyst	Overpotential (mV)	Electrolyte	Substrate	Reference
MoN-Ni ₃ C@CFs	271	1M KOH	NF	Present work
Ni ₃ N@NiMoN	317	1M KOH	NF	[5]
NiMoN@NiFeN	227	1M KOH	NF	[6]
CoN	290	1M KOH	NF	[7]
NiCo ₂ N/NF	290	1M KOH	NF	[8]
Ni ₃ ZnCo _{0.7} /NCNT	380	1M KOH	NF	[9]
HfN	358	1M KOH	NF	[10]
CoN _x /NGA	295	1M KOH	NF	[11]
V-Ni _{0.2} Mo _{0.8} N	245	1M KOH	NF	[12]
Mn ₃ N ₂	270	1M KOH	NF	[13]
FexN	238	1M KOH	NF	[14]
CoMo ₃ N	850	1M KOH	NF	[15]
Co-N _x -C	241	1M KOH	NF	[16]
NiMoN-450	260	1M KOH	NF	[17]
NSPM-Ni ₃ FeN	223	1M KOH	NF	[18]
NiMo _x C/NC-100	328	1M KOH	NF	[19]
CoMo ₂ C@NCT	377	1M KOH	NF	[20]
NiC/Mo ₂ C@C	258	1M KOH	NF	[21]
Co ₃ Mo ₃ C/Co@C	340	1M KOH	NF	[22]
Ni/Ni ₃ C	350	1M KOH	NF	[23]
Co-Ni ₃ C/Ni@C	325	1M KOH	NF	[24]
Ni ₃ C/NC	309	1M KOH	NF	[25]

Table S2. Comparison of HER performance of MoN-Ni₃C@CFs with recently reported transition metal-based catalysts

Catalyst	Overpotential (mV)	Electrolyte	Substrate	Reference
MoN-Ni ₃ C@CFs	132	1M KOH	NF	Present work
NiCo ₂ N	180	1M KOH	NF	[8]
Ni ₃ ZnCo _{0.7} /NCNT	203	1M KOH	NF	[9]
Fe ₃ C-GNRs	166.6	1M KOH	NF	[26]
FeC	154	1M KOH	NF	[27]
Ni-VC@C	146	1M KOH	NF	[28]
C/N-Mo ₂ C	197.7	1M KOH	NF	[29]
Mo ₂ C/W ₂ C	133	1M KOH	NF	[30]
Mo ₂ C-C	151	1M KOH	NF	[31]
Ni-Mo ₂ C-PC	179	1M KOH	NF	[32]
MoC-MoP/BCNC NFs	158	1M KOH	NF	[33]
Mo ₂ C-Mo ₂ N	205	1M KOH	NF	[34]
Mo ₂ C-NC	217	1M KOH	NF	[35]
P-MoN@NCN	181	1M KOH	NF	[36]
Ni/MoN@NCN	207	1M KOH	NF	[37]
NiFe ₃ N	158	1M KOH	NF	[38]
Mo ₂ N	353	1M KOH	NF	[39]
NiCoN	145	1M KOH	NF	[40]
Co _{5.47} N@N-C	149	1M KOH	NF	[41]
Co-Ni ₃ N	194	1M KOH	NF	[42]
Ni ₃ N	185	1M KOH	NF	[43]

Table S3. Comparison of overall water splitting performance of MoN-Ni₃C@CFs with recently reported transition metal-based catalysts

Catalyst	Voltage (η_{10})	Reference
MoN-Ni ₃ C@CFs	1.56	Present work
C ₃ N ₄ /NiCoP/NF	1.70	[44]
CuCo ₂ N _x /CF	1.70	[45]
Mo ₂ TiC ₂ T _x	1.57	[46]
Fe ₃ C/NC-550	1.57	[47]
N-Nb ₄ C ₃ T _x /NGC	1.58	[48]
β -Mo ₂ C	1.65	[49]
P-Fe ₃ N@NCNSs/NF	1.61	[50]
PdP ₂ @CB	1.72	[51]
CoP@NCNFs	1.59	[52]
V _{0.28} Co _{2.72} C/CNFs	1.60	[53]
Co-BM-C	1.60	[54]
CoP/Mo ₂ CT _x	1.58	[55]

Reference

1. T. S. Mathis, N. Kurra, X. Wang, D. Pinto, P. Simon, and Y. Gogotsi, *Adv. Energy Mater.* **2019**, 9, 1902007
2. A. Grimaud, O. Diaz-Morales, B. Han, W. T. Hong, Y.-L. Lee, L. Giordano, K. A. Stoerzinger, M. T. M. Koper, and Y. Shao-Horn, *Nat. Chem.* **2017**, 9, 457-465.
3. J. Saha, D. R. Chowdhury, P. Jash, and A. Paul, *Chem.-Eur. J.* **2017**, 23, 12519-12526.
4. C. Yang, C. Laberty-Robert, D. Batuk, G. Cibin, A. V. Chadwick, V. Pimenta, W. Yin, L. Zhang, J.-M. Tarascon and A. Grimaud, *J. Phys. Chem. Lett.*, **2017**, 8, 3466-3472.
5. B. Chang, Y. Zhong, Z. Ai, J. Zhang, D. Shi, K. Zhang, Y. Shao, J. Shen, B. Huang, L. Zhang and Y. Wu, *J. Chem.*, 2019, **43**, 14701-14707.
6. L. Yu, Q. Zhu, S. Song, B. McElhenny, D. Wang, C. Wu, Z. Qin, J. Bao, Y. Yu, S. Chen and Z. Ren, *Nat. Commun.*, 2019, **10**, 5106-5113.
7. Y. Zhang, B. Ouyang, J. Xu, G. Jia, S. Chen, R. S. Rawat and H. J. Fan, *Angew. Chem. Int. Ed. Engl.*, 2016, **55**, 8670-8674.

8. Y. Wang, B. Zhang, W. Pan, H. Ma and J. Zhang, *ChemSusChem*, 2017, **10**, 4170-4177.
9. R. Li, X. Li, D. Yu, L. Li, G. Yang, K. Zhang, S. Ramakrishna, L. Xie and S. Peng, *Carbon*, 2019, **148**, 496-503.
10. C. Defilippi, D. V. Shinde, Z. Dang, L. Manna, C. Hardacre, A. J. Greer, C. D'Agostino and C. Giordano, *Angew. Chem.*, 2019, **131**, 15610-15616.
11. H. Zou, G. Li, L. Duan, Z. Kou and J. Wang, *Appl. Catal. B: Environ.*, 2019, **259**, 118100-118112.
12. P. Zhou, X. Lv, D. Xing, F. Ma, Y. Liu, Z. Wang, P. Wang, Z. Zheng, Y. Dai and B. Huang, *Appl. Catal. B: Environ.*, 2020, **263**, 118330-118345.
13. C. Walter, P. W. Menezes, S. Orthmann, J. Schuch, P. Connor, B. Kaiser, M. Lerch and M. A. Driess, *Angew Chem.*, 2018, **130**, 706-710.
14. F. Yu, H. Zhou, Z. Zhu, J. Sun, R. He, J. Bao, S. Chen and Z. Ren, *ACS Catal.*, 2017, **7**, 2052-2057.
15. Y. Yuan, S. Adimi, T. Thomas, J. Wang, H. Guo, J. Chen, J. P. Attfield, F. J. DiSalvo and M. Yang, *Innov.*, 2021, **2**, 100096-100105.
16. C. Tang, B. Wang, H. F. Wang and Q. Zhang, *Adv mater.*, 2017, **29**, 1703185-1703197.
17. Z. Yin, Y. Sun, C. Zhu, C. Li, X. Zhang and Y. Chen, *J. Mater. Chem. A*, 2017, **5**, 13648-13658.
18. Y. Wang, C. Xie, D. Liu, X. Huang, J. Huo and S. Wang, *ACS appl. Mater. interfaces*, 2016, **8**, 18652-18657.
19. D. Das, S. Santra and K. K. Nanda, *ACS appl. Mater. interfaces*, 2018, **10**, 35025-35038.
20. X. Yin, L. Yang and Q. Gao, *Noble-Metal-Free Electrocatal. Hydrog. Energy*, 2022, **7**, 323-350.

21. K. Santhosh Kumar, D. Thiruvengadam, K. Rajan, R. Nithiasri and J. Jayabharathi, M. Padmavathy, *ACS Appl. Electron. Mater.*, 2024, DOI: 10.1021/acsaelm.4c01909
22. S. Gao, L. Lin, H. Wang, P. Nie, J. Jian, J. Li and L. Chang, *J. Alloys Compd.*, 2021, **875**, 160052-160064.
23. Q. Qin, J. Hao and W. Zheng, *ACS appl. Mater. interfaces*, 2018, **10**, 17827-17834.
24. X. Jia, M. Wang, G. Liu, Y. Wang, J. Yang and J. Li, *Int. J. Hydrog. Energy*, 2019, **44**, 24572-24579.
25. X. Wang and M. Sun, *Int. J. Electrochem. Sci.*, 2021, **16**, 210530-210544.
26. S. Li, J. Yang, C. Song, Q. Zhu, D. Xiao and D. Ma, *Adv. mater.*, 2019, **31**, 1901796-1901806.
27. X. Fan, Z. Peng, R. Ye, H. Zhou and X. Guo, *ACS Nano*, 2015, **9**, 7407-7418.
28. L. Peng, J. Shen, L. Zhang, Y. Wang, R. Xiang, J. Li, L. Li and Z. Wei, *J. Mater. Chem. A*, 2017, **5**, 23028-23034.
29. R. A. Mir and O. P. Pandey, *RSC Sustainable Energy Fuels*, 2020, **4**, 655-669.
30. Y. Ling, F. M. Kazim, Q. Zhang, S. Xiao, M. Li and Z. Yang, *Int. J. Hydrog. Energy*, 2021, **46**, 9699-9706.
31. J. Li, C. Zhang, C. Wu, Y. Liu, X. Zhang, X. Li, Y. Li, J. Sun and Z. Su, *Chin. Chem. Lett.*, 2024, **35**, 108782-108795.
32. Z. Y. Yu, Y. Duan, M. R. Gao, C. C. Lang, Y. R. Zheng and S. H. Yu, *Chem. sci.*, 2017, **8**, 968-973.
33. N. Chen, Q. Mo, L. He, X. Huang, L. Yang, J. Zeng and Q. Gao, *Electrochim. Acta*, 2019, **299**, 708-716.
34. X. Chen, J. Qi, P. Wang, C. Li, X. Chen and C. Liang, *Electrochim. Acta*, 2018, **273**, 239-247.
35. Y. J. Song and Z. Y. Yuan, *Electrochim. Acta*, 2017, **246**, 536-543.

36. C. Wang, X. Lv, P. Zhou, X. Liang, Z. Wang, Y. Liu, P. Wang, Z. Zheng, Y. Dai, Y. Li and M. H. Whangbo, *ACS Appl. Mater. Interfaces*, 2020, **12**, 29153-29161.
37. B. M. Hunter, H. B. Gray and A. M. Muller, *Chem. Rev.*, 2016, **116**, 14120-14136.
38. X. Jia, Y. Zhao, G. Chen, L. Shang, R. Shi, X. Kang, G. I. Waterhouse, L. Z. Wu, C. H. Tung and T. Zhang, *Adv. Energy Mater.*, 2016, **6**, 1502585-1502598.
39. M. Shalom, D. Ressnig, X. Yang, G. Clavel, T. P. Fellingner and M. Antonietti, *J. Mater. Chem. A*, 2015, **3**, 8171-8184.
40. L. Han, K. Feng and Z. Chen, *Energy Technol.*, 2017, **5**, 1908-1911.
41. Z. Chen, Y. Ha, Y. Liu, H. Wang, H. Yang, H. Xu, Y. Li and R. Wu, *ACS Appl. Mater. Interfaces*, 2018, **10**, 7134-7144.
42. C. Zhu, A. L. Wang, W. Xiao, D. Chao, X. Zhang, N. H. Tiep, S. Chen, J. Kang, X. Wang, J. Ding and J. Wang, *Adv. Mater.*, 2018, **30**, 1705516-1705528.
43. M. Ledendecker, H. Schlott, M. Antonietti, B. Meyer and M. Shalom, *Adv. Energy Mater.*, 2017, **7**, 1601735-1601750.
44. S. Xu, Y. Feng, J. Bai, X. Sun and C. Li, *J. Alloys Compd.*, 2024, **1005**, 176151-176164.
45. Z. Kayış and D. Akyüz, *Phys. Chem. Chem. Phys.*, 2020, **26**, 14908-14918.
46. S. A. Zahra, M. W. Hakim, M. A. Mansoor and S. Rizwan, *Electrochim. Acta*, 2022, **434**, 141257-141269.
47. W. Guo, J. Li, D. F. Chai, D. Guo, G. Sui, Y. Li, D. Luo and L. Tan, *Adv. Sci.*, 2024, **5**, 2401455-2401467.
48. C. Xu, F. Wu, C. Hu, L. Yang and S. Yin, *J. Alloys Compd.*, 2024, **1004**, 175837-175848.
49. J. Xing, Y. Li, S. Guo, T. Jin, H. Li, Y. Wang and L. Jiao, *Electrochim. Acta*, 2019, **298**, 305-312.
50. G. Li, J. Yu, W. Yu, L. Yang, X. Zhang, X. Liu, H. Liu and W. Zhou, *Small*, 2020, **16**, 2001980-2001991.

51. F. Luo, Q. Zhang, X. Yu, S. Xiao, Y. Ling, H. Hu, L. Guo, Z. Yang, L. Huang, W. Cai and H. Cheng, *Angew. Chem. Int. Ed.*, 2018, **57**, 14862-14867.
52. L. Zhi, J. Tu, J. Li, M. Li and J. Liu, *J. Colloid Interface Sci.*, 2022, **616**, 379-388.
53. S. Zhang, G. Gao, J. Hao, M. Wang, H. Zhu, S. Lu, F. Duan, W. Dong, M. Du and Y. Zhao, *ACS Appl. Mater. Interfaces*, 2019, **11**, 43261-43269.
54. T. L. Jin, X. Liu, Q. Gao, H. Zhu, C. Lian, J. Wang, R. Wu and Y. Lyu, *Chem. Eng. J.*, 2022, **433**, 34089-34096.
55. S. Liu, Z. Lin, R. Wan, Y. Liu, Z. Liu, S. Zhang, X. Zhang, Z. Tang, X. Lu and Y. Tian, *J. Mater. Chem. A*, 2021, **9**, 21259-21269.